Apparatus to measure simultaneously 14 isometric leg joint moments. Part 1: Design and calibration of six-axis transducers for the forces and moments at the ankle

N. de N. Donaldson[1] M. Munih[2] T. A. Perkins[1] D. E. Wood[3]

[1]Department of Medical Physics & Bioengineering, University College London, London, UK

[2]Faculty of Electrical Engineering, University of Ljubljana, Ljubljana, Slovenia

[3]Department of Medical Physics & Biomedical Engineering, Salisbury District Hospital, Salisbury, UK

Abstract—*An apparatus has been developed for making isometric measurements of the joint moments corresponding to the 14 degrees of freedom of the legs, in postures ranging between sitting and near full extension. The apparatus is called the multi-moment chair system (MMCS) and is described in the companion paper. This paper describes the most critical components of the MMCS, which are the six-axis transducers for measuring the force and moment components on the plantar-flexion axis of each ankle while the feet are laced into fixed shoes. The transducers are made of steel bars, on which strain gauges are mounted, joined by clamps. The design of the transducer and methods of calibration and error estimation are described. The RMS errors are less than 2 N for the forces and 1 Nm for the moments, but these may be correlated. A method for error reduction that compensates for the finite compliance of the transducer does not reduce the measured errors.*

Keywords—*LARSI, Isometric contractions, Force transducer, Six-axis*

Med. Biol. Eng. Comput., 1999, **37**, 137–147

1 Introduction

IF ELECTRICAL stimulation is to be used to restore function following spinal cord injury, there are compelling arguments for using implanted stimulators. With few external unattractive wires, the system should always be ready for use. More muscles can be stimulated, so that more normal movements with less fatigue should be possible.

Some encouraging results have been reported (WILEMON *et al.*, 1970; BRINDLEY *et al.*, 1979; THOMA *et al.*, 1983; DONALDSON, 1986; DAVIES *et al.*, 1995); however, the question of the best site or sites for the electrodes remains unresolved. Conceptually the most straightforward approach is to place the electrodes towards the periphery, close to the target muscles, so that the direct (i.e. non-reflex) effects of stimulating each electrode are predictable. However, poor reliability and the extensive surgery required are important disadvantages of this option (RUSHTON, 1990).

We are now implanting stimulators of the lumbar anterior roots into volunteer paraplegics. The lumbar electrode books are similar in construction to those with three slots used for sacral anterior root stimulation, to restore micturition following spinal cord injury. Documented evidence from 500 patients with sacral root stimulators shows that intra-dural electrodes can be very reliable (BRINDLEY, 1995), and we hope that devices with a greater number of channels (12) for leg function will also be reliable.

Siting the electrodes at this more central location brings a concomitant difficulty. From anatomy, it is known broadly from which anterior roots each leg muscle is innervated (GRAY, 1989). LIGUORI *et al.* (1992) investigated sensory and motor innervation from the spinal nerves (L2-S2) using percutaneous needles. HAMSTER (1995) studied the EMG responses of six major muscles bilaterally to acute stimulation of the L4-S2 roots in eight subjects, during laminectomy operations that exposed the lumbar roots. Evidently, the effect of the stimulation of each root is to cause many muscles to contract, possibly in a synergistic manner (RUSHTON, 1990). However, none of the information provided by these studies is specific enough to allow the responses to root stimulation to be exactly predicted at all the joints, whether the roots are stimulated singly or in combination. It is also clear that there will be considerable individual variation that will have to be taken into account in setting up the stimulation system for each user. To find out what combinations of stimulation intensities are optimum for each individual, the responses at the joints to combined-root stimulation must be measured.

Tension in the leg muscles causes moments at the joints that may result in motion. It is an inconvenient fact, when we wish to characterise the effect of root stimulation, that the muscle tensions depend not only on the stimulation of one or more

Correspondence should be addressed to Dr N. de N. Donaldson; email: nickd@medphys.ucl.ac.uk

First received 27 October 1997 and in final form 2 November 1998

roots, but also on the muscles' state of fatigue and potentiation, and on the joint angles and their velocities. There may also be reflex effects of stimulation, but, as we are stimulating anterior roots, which are predominantly motor fibres, we expected the reflex effects to be small. (We have found that this assumption was optimistic. Reflex responses during lumbar anterior root stimulation will be the subject of a forthcoming paper.) Because we are chiefly interested in using the implant for standing, with muscles contracting without significant movement, we decided to measure the isometric responses at several possible positions of the body, between a seated posture and close to full extension of the knees and hips, and to restrict the range of postures to those with equal extension in both legs.

Added to the muscle activity (and resulting joint moments) due to nerve root stimulation, is muscle activity due to the endogenous activity of the severed spinal cord. This endogenous activity can depend on whether the subject is bearing weight on their feet (supporting reaction (CARPENTER, 1996)) and on any irritant sensory inputs, such as pinching shoes. However, given the time that these measurements necessarily take, we decided that we could not begin with the subject upright. To be practicable, we would measure the joint moments while the body was in an extended posture but recumbent.

We therefore arrived at the notion of a laboratory measurement system, in which the subject sits and which can recline like a dentist's chair. The trunk and legs are fixed in the required posture, and then stimulation is applied. The fixation allows little movement, so that the time taken for the limbs to stop moving is short. Consequently, rapid measurements are possible (about 5 s per stimulation pattern) and so many measurements can be made before the muscles become very fatigued. Many measurements are necessary to find even an approximate relationship between the stimulation intensities and the joint moments, because, even for one side of the body, this is a 6D–7D mapping.

We call this apparatus the multi-moment chair system (MMCS), and it is the subject of this pair of papers. The system requires the three forces and three moments between the foot and the foot's fixation. We do this by tying the foot into a shoe that itself is glued to a plate that, in turn, is bolted to the base of a footbox. Each footbox is supported by bilateral bearings aligned with the ankle plantar-flexion axis. When the plantar-flexion angle has been set, the box is clamped in place.

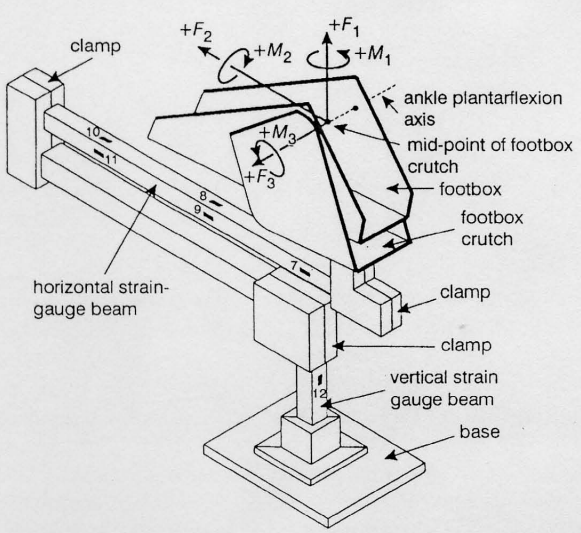

Fig. 1 *Six-axis ankle transducer that restrains left foot, viewed from behind and left. Ankle plantar-flexion axis is 545 mm above bottom surface of base, and overall length is 674 mm. Transducer is orientated with horizontal beams pointing away from seat (see Fig. 2 in Part 2)*

It is convenient to measure the fixation forces on the line of the plantar-flexion axis, as shown in Fig. 1. From these signals and also force signals from the knee supports, it is possible to calculate the joint moments from consideration of static equilibrium of parts of the leg.

This paper describes the design, calibration and measurement of accuracy of the six-axis 'ankle' force transducers. The companion paper describes the remainder of the MMCS and considers the overall errors that can be expected in calculating the 14 joint moments.

Although 'six-axis' load cells can be bought, they are expensive (perhaps £4000). On the other hand, literature that describes the design, calibration and performance of such transducers is scarce (however, see BOYLE (1992) and PERRY *et al.* (1992)). We were not constrained to make these transducers small, as is often the case. Instead, we chose to use a large but simple beam structure to carry the strain gauges, the beams being joined by mild steel clamps.

2 Design of the transducer

2.1 *Specification*

The axes used are the same for both transducers (Fig. 1): axis 1 is vertical upwards; axis 2 is longitudinal away from the seat; and axis 3 is lateral to the left, seen from the seat. Positive forces are those applied to the transducer, acting in these directions. Note that $+F_3$ tends to be produced by a hip adduction moment in the right leg or a hip abduction moment in the left.

Our original specification was rather cautious about the maximum loads that might be applied to the transducer (see Table 1). Since beginning to use the transducer, we have found that the leg joint moments are never large enough to cause these forces and moments. Also we have changed the multi-moment chair so that F_2 is never much greater than F_1. However, these large forces and moments were used to calculate the sizes of the transducer's parts.

2.2 *General considerations*

A cantilever can be subjected to bending strain by application of either a transverse force or a moment. To be able to distinguish, and therefore measure, both of these loads, the bending moment can be measured at two different sites along the beam. Application of a pure moment will put an equal bending moment all along the beam, whereas a pure transverse force will cause a triangular bending moment distribution. This is well known. By placing strain gauges on the orthogonal faces of a rectangular beam, the forces and moments can be measured for two perpendicular axes. The gauge sites should be well separated, as the force will be calculated from the difference in the bending moments.

Our transducer (Fig. 1) extends this idea so that the other two force–moment components can also be measured. The arrangement is not as straightforward as in the cantilever example, because the forces and moments are not applied at the end of the horizontal beam, but on the ankle axis above. This vertical distance results in sagging strain in the horizontal strain gauged beam if forces F_1 or F_2 or moment M_3 are applied.

By carrying the load back through the vertical beam to the base, where the vertical beam is below the point of application of the load, the bending moment at site 12 is independent of

Table 1 Specified maximum loads

F_1	F_2	F_3	M_1	M_2	M_3
±1000 N	±2000 N	±1500 N	±200 Nm	±200 Nm	±400 Nm

F_1, and therefore all three components can be calculated from the bending moments at sites 8, 10 and 12. M_2 only affects the torsion bridge in the horizontal beam at site 7. The lateral force F_3 affects both torsion at site 7 and the bending moments at sites 9 and 11. M_1 applies equal bending moment at sites 9 and 11. These statements imply that each force or moment can be calculated from the outputs of two of three channels. In fact, for a non-ideal transducer, there will be cross-talks, and so a more realistic representation is a 6×6 matrix relating the six bridge signals to the six forces and moments.

Unlike load cells, which are machined from solid, this transducer uses clamps to join the horizontal and vertical bars. These clamps will cause local distortion of the strain field. To avoid measurement errors due to these distortions, we mounted all the strain gauges at least two bar widths away from the nearest clamp.

The transducer is to be used only in differential mode. When the subject is sitting in the apparatus, with some weight resting on the transducer, the amplifier output voltages are recorded. These 'offsets' are then subtracted from all subsequent readings, and the differences are used as the bridge outputs, corresponding to the additional forces and moments that are subsequently applied to the transducer. The assumption is that the transducer is linear, and therefore that the calculation matrix can be applied for such 'difference' voltages. During calibration (Section 3), the analogous procedure is to arrange the transducer, orientated correctly for the next loading, and then take offsets. Thereafter, changes in the voltages are measured as successive weights are added. The absolute voltages are never used.

2.3 *Design*

The three long bars are a nickel-molybdenum case-hardening steel (type EN34 according to BS970), which was not heat treated. This material was chosen because of its high elastic limit (Young's modulus 200 GPa; yield strength 680 MPa). The flats for the gauges were ground and finished with metal polish to give a very smooth surface for bonding.

The gauge foils at sites 8–12 (type EA-06-250MQ-350), for measuring bending strain, have two elements parallel to the long axis of the bar, and the foils were bonded on opposite faces. At site 7, each foil had a 90° rosette (type CEA-06-062UR-350), inclined at 45° to measure torsion: again, each of a pair of foils was mounted on opposite faces*.

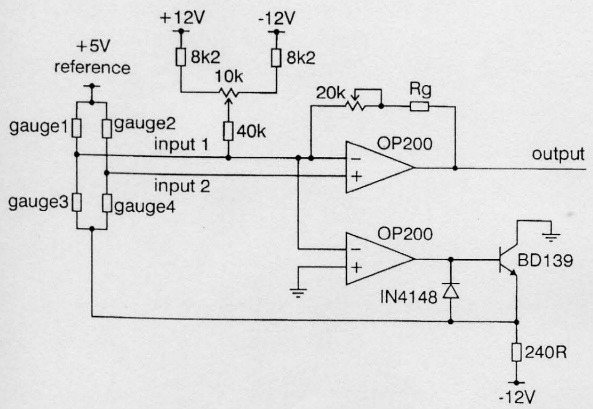

Fig. 2 *Schematic diagram of one amplifier. All strain gauges are 350Ω. See Table 1 for measured values of total feedback resistance*

*From the Measurement Group, Basingstoke, Hants, RG24 0QA, UK

Table 2 Values of gain-setting resistors for amplifiers

Channel	Feedback resistance, kΩ (R_g + part of 20 kΩ preset)
7	36.4
8	37.9
9	66.6
10	35.3
11	44.7
12	37.5

Each bridge has a differential amplifier, with a design based on that presented by SHELL (1990) (Fig. 2). The gains of these amplifiers have been set according to the bridge sensitivities; these settings are recorded in Table 2 by the measured values of the total feedback resistance for each amplifier.

The power supply current for each amplifier is 26 mA. There are 18 amplifiers, together drawing 468 mA from the positive power rail. The power supply has a rated ripple of 6 mV, with regulation of 40 mV from nought to maximum load current, and 10 mV for the full range of mains voltage. (The power supply has two RS Components type 591-253, set to 12 V, giving ±12 V rails. Each is rated for 1 A.)

2.4 *Estimation of the inverse matrix*

When the transducer is in use, a matrix in the MMCS program calculates the three components of force and the three components of moment from the six voltage differences that appear at the outputs of the strain gauge amplifiers.

$$\begin{bmatrix} F_1 \\ F_2 \\ F_3 \\ M_1 \\ M_2 \\ M_3 \end{bmatrix} = \begin{bmatrix} g_{11} & g_{12} & g_{13} & g_{14} & g_{15} & g_{16} \\ g_{21} & g_{22} & g_{23} & g_{24} & g_{25} & g_{26} \\ g_{31} & g_{32} & g_{33} & g_{34} & g_{35} & g_{36} \\ g_{41} & g_{42} & g_{43} & g_{44} & g_{45} & g_{46} \\ g_{51} & g_{52} & g_{53} & g_{54} & g_{55} & g_{56} \\ g_{61} & g_{62} & g_{63} & g_{64} & g_{65} & g_{66} \end{bmatrix} \begin{bmatrix} V_{\#7} \\ V_{\#8} \\ V_{\#9} \\ V_{\#10} \\ V_{\#11} \\ V_{\#12} \end{bmatrix}$$

$$\boldsymbol{F} = \boldsymbol{G}.\boldsymbol{V} \tag{1}$$

This applies to the right ankle transducer, which is connected to amplifiers 7–12. However, to estimate the coefficients g_{ij}, it is easier to work with the 'inverse' matrix $\boldsymbol{K}$

$$\boldsymbol{V} = \boldsymbol{K}.\boldsymbol{F} \tag{2}$$

$\boldsymbol{K}$ can be estimated by finding four groups of factors: the bending moments or torque in the beams at the gauge sites due to the six components of $\boldsymbol{F}$ (6×6 matrix); the six stiffnesses at the sites (surface strain per Nm); the six bridge sensitivities (fractional change per unit strain); and the amplifier gains (volts out per unit fractional change). The fractional change means the change in the proportion of the voltage across the bridge that appears at the amplifier input.

2.4.1 *Moments in the beams:* By inspection of Fig. 3, we can see how the moments at the six gauge sites depend on the three forces and three moments applied at the middle of the ankle joint. The matrix (eqn. 3) has the lever arms of the externally applied forces in the left half, expressed in metres, and, in the right half, are numbers that describe whether the externally applied moments do or do not exert internal torque or bending moment.

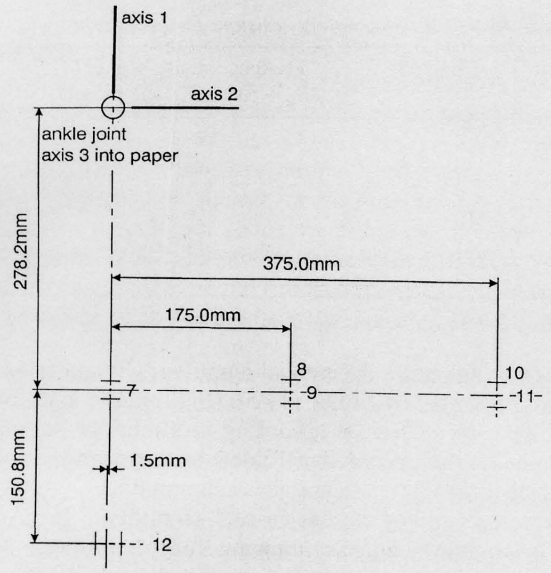

Fig. 3 *Dimensions of transducer and positive directions of axes. Right ankle transducer for MMCS. View from lateral side. Numbers correspond to bridge sites. Mid-point of footbox crutch is 7.5 mm on lateral side of plane of beams*

$$\begin{bmatrix} T_7 \\ M_8 \\ M_9 \\ M_{10} \\ M_{11} \\ M_{12} \end{bmatrix} = \begin{bmatrix} 0.0075 & 0 & -0.278 & 0 & 1 & 0 \\ 0.175 & 0.278 & 0 & 0 & 0 & 1 \\ 0 & 0 & -0.175 & 1 & 0 & 0 \\ 0.375 & 0.278 & 0 & 0 & 0 & 1 \\ 0 & 0 & -0.375 & 1 & 0 & 0 \\ 0 & -0.429 & 0 & 0 & 0 & -1 \end{bmatrix} \begin{bmatrix} F_1 \\ F_2 \\ F_3 \\ M_1 \\ M_2 \\ M_3 \end{bmatrix} \quad (3)$$

where T_7 is the torque at site 7, and the M_n are bending moments at sites 8–12. An arbitrary sign convention has been used. If we call displacements of the transducer's ankle joint x_1, x_2, x_3, θ_1, θ_2 and θ_3, then a positive torque or a positive bending moment will cause displacements as shown in Table 3.

2.4.2 *Stiffnesses:* At site 7, the beam is 17.5 mm square. According to YOUNG (1989) (p. 348), for a square shaft in torsion, the maximum shear stress, which occurs at the midline of each face, lies parallel to the long axis. An equal shear stress occurs on the perpendicular line across each face. Under this stress loading, the principal (i.e. direct) stresses (σ_x, σ_y) run at 45° and are of the same magnitude (YOUNG, 1989) (p. 85).

$$\sigma_x = -\sigma_y = \frac{0.601 \times T}{a^3} \quad (4)$$

Table 3 Sign convention for strain at gauge sites. Displacement by rotation (θ) or translation (x) in direction given in second column gives positive strain signal at corresponding gauge site

Gauge site	Displacement
7	$+\theta_2$
8	$+x_1$
9	$-x_3$
10	$+x_1$
11	$-x_3$
12	$-x_2$

Table 4 Bending stiffnesses of beams at gauge sites

Site	b, mm	d, mm	ε/M, $(\text{Nm})^{-1}$
8	23.5	23.5	2.31×10^{-6}
9	23.5	23.5	2.31×10^{-6}
10	25.5	25.5	1.81×10^{-6}
11	25.5	25.5	1.81×10^{-6}
12	26.5	25.0	1.81×10^{-6}

where the width of the bar is $2a$. Because of the bi-directional stresses, the strains depend on Poisson's ratio v

$$E\varepsilon_x = \sigma_x - \upsilon\sigma_y = \sigma_x(1 + v) \quad (5)$$

$$E\varepsilon_y = \sigma_y - \upsilon\sigma_x = \sigma_y(1 + v) \quad (6)$$

E is Young's modulus. The maximum direct stress is $\sigma_{max} = |\sigma_x| = |\sigma_y|$, and the maximum direct strain ε_{max} is

$$E\varepsilon_{max} = \pm\sigma(1 + v) \quad (7)$$

$$\varepsilon_{max} = \frac{0.601 \times T \times (1 + v)}{E \times a^3} \quad (8)$$

Using $v_{steel} = 0.3$ and $E = 200$ GPa, and given that $a = 8.75$ mm, $\varepsilon_{max}/T = 5.83 \times 10^{-6}$ $(\text{Nm})^{-1}$.

For a rectangular beam, width b and depth d, the second moment of area is $I = bd^3/12$. The longitudinal surface strain is given by

$$\varepsilon = \frac{Md}{2EI} = \frac{6M}{Ebd^2} \quad (9)$$

and thus, at sites 8–12, the stiffnesses are as given in Table 4.

2.4.3 *Bridge sensitivities:* All the Wheatstone bridges have four active arms; for bridge 7, the strain gauge elements are aligned at 45°, and for bridges 8–12, the elements all lie parallel to the long axis of the beams. If the gauge factor for the foil gauges is 2.1, then, for every microstrain change, each gauge will change by 2.1×10^{-6}. The change in the bridge output voltage, as a fraction of the supply voltage to the bridge, will also be 2.1×10^{-6}.

2.4.4 *Amplifier gains:* The amplifiers were calibrated with a dummy bridge in which the three-way two-pole switch allows the high-value shunt resistors to unbalance the bridge equally in either way. The shunt resistance can be set to one, two or three 1 MΩ resistors in parallel. The greatest change in output occurs with all three together (i.e. 333 kΩ, as shown in Fig. 4).

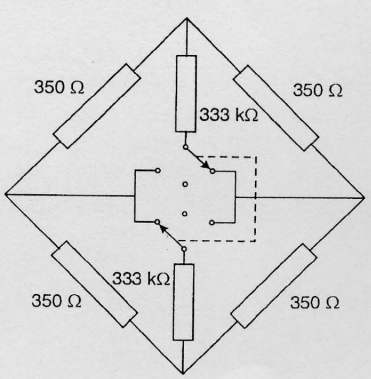

Fig. 4 *Bridge for calibrating amplifier gains. Bridge resistors are 0.1%*

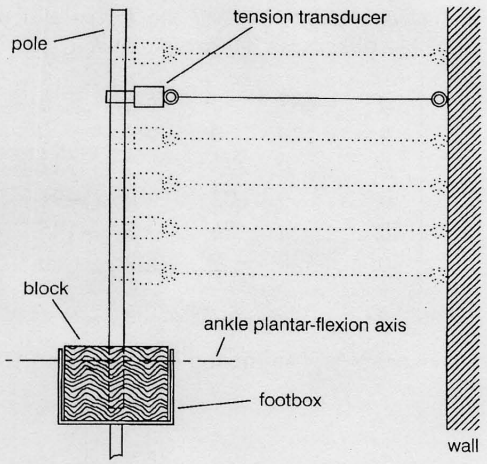

Fig. 5 *Offset loading. A force of nominally the same value is applied horizontally to the pole at 10 cm intervals*

eqn. 11 is

$$\begin{bmatrix} V_7 \\ V_8 \\ V_9 \\ V_{10} \\ V_{11} \\ V_{12} \end{bmatrix} = \begin{bmatrix} k_{11} & k_{12} & k_{13} & k_{14} & k_{15} & k_{16} \\ k_{21} & k_{22} & k_{23} & k_{24} & k_{25} & k_{26} \\ k_{31} & k_{32} & k_{33} & k_{34} & k_{35} & k_{36} \\ k_{41} & k_{42} & k_{43} & k_{44} & k_{45} & k_{46} \\ k_{51} & k_{52} & k_{53} & k_{54} & k_{55} & k_{56} \\ k_{61} & k_{62} & k_{63} & k_{64} & k_{65} & k_{66} \end{bmatrix} \begin{bmatrix} F_1 \\ F_2 \\ F_3 \\ M_1 \\ M_2 \\ M_3 \end{bmatrix} \quad (13)$$

If, for example, only F_1 is changed, we can differentiate with respect to F_1 to obtain $dV_7/dF_1 = k_{11}$, $dV_8/dF_1 = k_{21}$ etc. In other words, the elements of $\boldsymbol{K}$ are the slopes when the channel voltage is plotted against the changing load.

3.3 *Amplifier linearity*

Linearity of the amplifiers was tested using the calibrator shown in Fig. 4. Using only the 333 kΩ shunts, each amplifier was tested at three input conditions. With all the amplifiers adjusted so that, with the bridge in balance, the output offsets were approximately 0 V, the maximum deviation from a straight line response was ±3 mV. Two amplifiers were tested with their outputs offset by ±1 V: the deviation remained within 3 mV. Note that the change in output between the extreme out-of-balance conditions was variable (see Table 5), up to 3.95 V, and that the measurement was performed using the A–D converters, which were set with a range of ±2.5 V, so that the quantisation step was $5/4096 = 1.22$ mV.

3.4 *Results*

The results are plotted in Figs. 6 *a–f*. The 36 graphs show the slopes of all the coefficients k_{ij} in eqn. 13. On the graphs with responses to positive and negative loading, the voltages at the initial zero load for each direction of loading were taken as offsets. The best slope for each graph was determined by fitting a straight line to all the data points, so as to minimise the sum of the square of the differences (using MATLAB** 'polyfit'). These lines are shown in the Figure. Their slopes are the elements of $\boldsymbol{K}_{calib}$.

** Cambridge Control Ltd, Cambridge, UK

$$\boldsymbol{K}_{calib} = \begin{bmatrix} -0.130 & -0.122 & -7.106 & 0.788 & 26.66 & -0.481 \\ 1.833 & 3.002 & -0.083 & -0.318 & 0.077 & 11.09 \\ 0.039 & 0.123 & -3.114 & 18.70 & -0.769 & 0.255 \\ 3.091 & 2.308 & -0.053 & -0.381 & 0.101 & 8.491 \\ -0.018 & -0.014 & -4.041 & 10.66 & -0.003 & -0.061 \\ 0.098 & -3.840 & 0.146 & 0.206 & -0.231 & -9.162 \end{bmatrix} \quad (14)$$

The inverse of this matrix is what we want when using the transducer ($\boldsymbol{G}_{calib}$).

$$\boldsymbol{G}_{calib} = \begin{bmatrix} -0.8 & -448.0 & 4.8 & 589.0 & -0.7 & 3.9 \\ -5.5 & -1139.4 & 8.3 & 698.8 & -9.0 & -730.9 \\ 7.7 & 7.9 & 264.2 & -10.7 & -4464.3 & 9.7 \\ 2.9 & 3.4 & 100.2 & -3.8 & -82.2 & 3.8 \\ 39.5 & 3.1 & 67.5 & -1.8 & -121.4 & 2.7 \\ 1.5 & 472.9 & 1.4 & -286.7 & -2.4 & 197.4 \end{bmatrix} \quad (15)$$

4 Estimation of accuracy

4.1 *Loading to test the calibration*

To estimate the accuracy of the transducer, using the calibration matrix $\boldsymbol{G}_{calib}$, the transducer was loaded with combined forces and moments, as described in Table 7. A light plank was bolted to the transducer footbox, on which was mounted a wooden block and a vertical pole. Vertical forces were applied by placing a weight on the plank. Horizontal forces were applied by pulling horizontally on the pole, with a rope attached to the ATP Instruments balance.

4.2 *Errors using calibration matrix*

The forces and moments were calculated using the matrix $\boldsymbol{G}_{calib}$ from the amplifier voltages. They were subtracted from the applied forces and moments (Table 6) to give errors that are plotted for the 69 loads in Fig. 7. The solid lines are these errors, which have been separated into the 11 loading groups.

The RMS values of the six errors, averaged over all 69 tests, are given in Table 8. If we regard the errors as random (or at least not systematic), these errors can be regarded as the expected standard deviations for the measurements.

5 Discussion

5.1 *Difficulties encountered during calibration*

Calibration was much more difficult than expected, and the satisfactory results shown here were only achieved after many attempts. We originally chose to apply couples to the transducer for moment calibration. Fig. 8 shows how we did this for M_2 calibration. M_1 and M_3 had similar arrangements, with wires applying tension in opposing directions, but more pulleys were used to arrange both wires to pull horizontally. The essential idea was that equal and opposite forces were applied, because the suspended bar shared the weight between the two wires. However, the tensions in the wires close to the transducer are only equal to half W if there is no friction in the pulleys, and, to

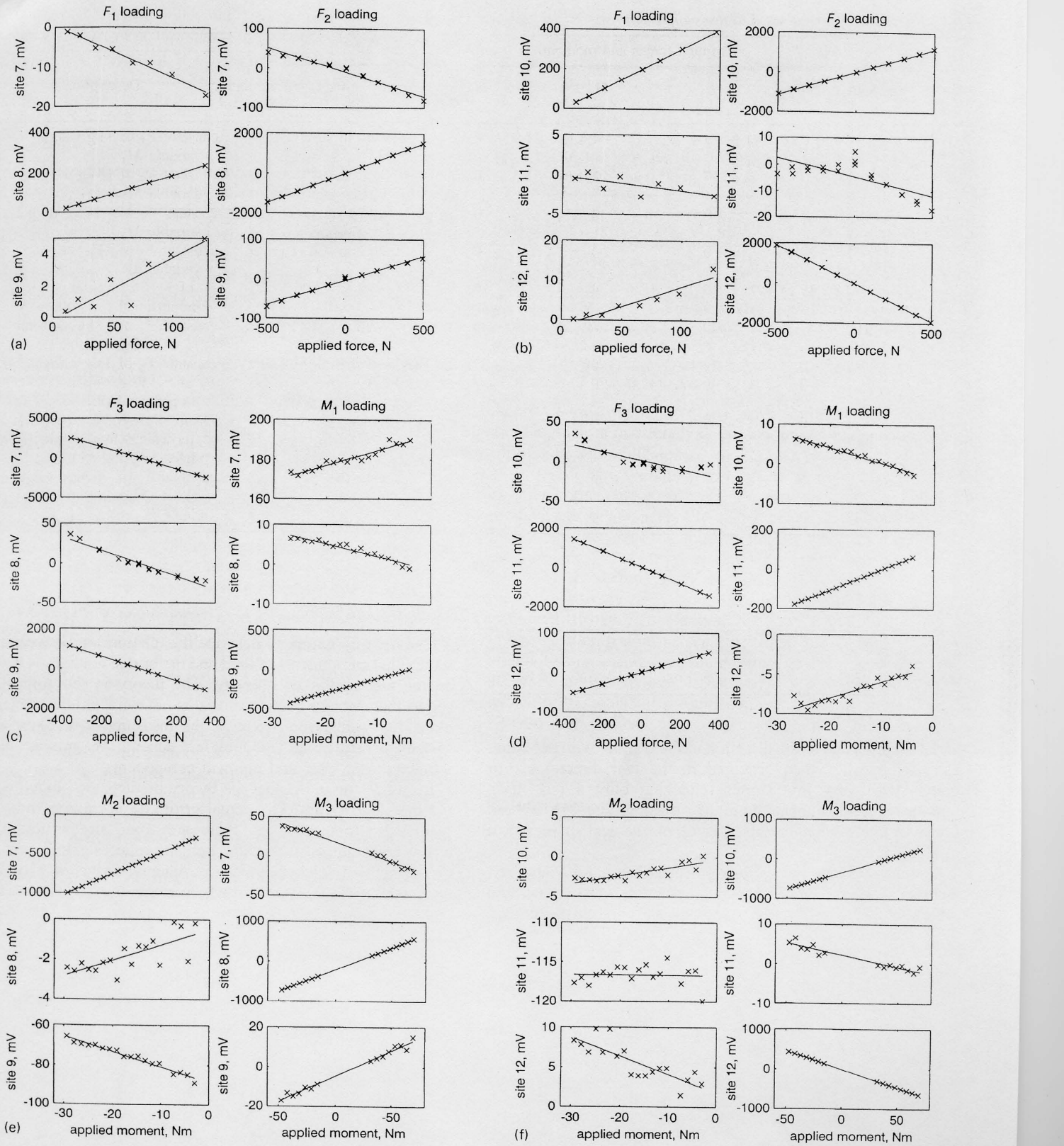

Fig. 6 *Six channel outputs for all six loadings. (X) Measured points; (——) straight line, fitted to data, with minimum square error. Slopes are numbers in matrix* $\boldsymbol{K}_{calib}$*: for example, in graph for site 7 with* F_1 *loading, slope is* $-0.130\,mV\,N^{-1}$

our surprise, even with pulleys running on ball races, there was significant friction. On one occasion, we found a 9% difference in the tension.

To obtain the results presented in this paper, we had to abandon loading with couples and use offset forces instead (i.e. a constant force applied with a varying leverage). Also, we had to measure the tension between the pulley and the transducer being calibrated with a tension transducer, rather than using calibrated dead weights.

If we relate the graphs of Fig. 6 to the corresponding elements of the matrix $\boldsymbol{K}_{theory}$ (eqn. 11), we see that all the elements that are not small or zero show linear responses. For example, the second column of $\boldsymbol{K}_{theory}$ has non-zero elements in the second, fourth and sixth rows, and the graphs for sites 8, 10 and 12, under F_2 loading in Fig. 6, are straight lines. The other F_2 loading graphs (sites 7, 9 and 11) should ideally be zero, but actually exhibit relatively small responses, and these are all more or less non-linear. Presumably, the change in slope

Table 7 Eleven loadings used to test calibration

Group	Applied forces and moments in group						Number of loads	Description
	F_1	F_2	F_3	M_1	M_2	M_3		
1	−1.4	0	−29.4	−4.4 to −27.9	0	0.2 to 1.3	9	constant F_3 of 3 kg weight, variable M_1
2	−1.4	0	−147	−22.0 to −51.5	0	0.2 to 0.48	3	constant F_3 of 15 kg weight, variable M_1
3	−106.4	0	0	0	0	69.2 to −47.9	8	constant F_1 of −11 kg weight, variable M_3
4	−2.8	29.4	0	0	0	29.7 to 4.4	9	constant F_2 of 3 kg weight, variable M_3
5	−2.8	49 to 147	0	0	0	7.4 to 22.0	3	F_2 of 5–15 kg weight, proportional variation of M_3
6	−109.2	147	0	0	0	98.6 to −18.5	8	constant F_1 of 11 kg, constant F_2 of 15 kg, variable M_3
7	−2.8	0	29.4	0	−27.9 to −4.4	0	9	constant F_3 of 3 kg, variable M_2
8	−2.8	0	49.0 to 147.0	0	−7.4 to −22.1	0	3	F_3 of 5–15 kg weight, proportional variation in M_2
9	−2.8	0	49.0	0	−17.2	0	1	F_3 of 5 kg weight, greater M_2 (recordings from 3 other loads deleted as outliers)
10	−109.2	0	147	0	−22.1	69.2 to −47.9	8	constant F_1 of −11 kg weight and F_3 of 15 kg, variable M_3
11	10 to 126.7	0	0	0	0	0	8	variable F_1

Table 8 RMS values of six errors averaged over all 69 tests

F_1	F_2	F_3	M_1	M_2	M_3
0.82 N	1.93 N	1.57 N	0.54 Nm	0.62 Nm	0.86 Nm

at the origin is due to the direction of the loading wire not being exactly opposite when arranged in the two directions. For graphs with very low slopes (changing only a few mV), random variations appear (e.g. M_2 loading, site 11): we did not investigate whether this was of mechanical or electrical origin.

Comparison of the calibration matrix eqn. 12 and the theoretical matrix eqn. 15, estimated from beam theory and properties of the gauges and amplifiers, shows good agreement.

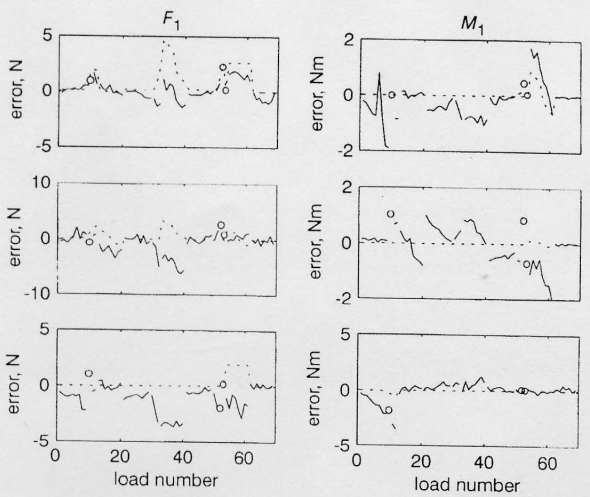

Fig. 7 *Error in forces and moments during application of 69 loads. (——) Errors predicted from theory presented in Appendix; is broken into segments, corresponding to 11 groups of loads (Table 6)*

5.2 *Systematic errors due to the compliance of transducer*

The use of a matrix to describe the relationship between the six applied components of load and the bridge voltages is based on the assumption of linearity. The theory in the Appendix shows that, for any transducer that is not rigid and that deflects under the load, errors occur in the measurements. These are systematic and their magnitudes depend on product and squares of the force and moment components.

In Fig. 7, the errors that the theory predicts are plotted with the measured errors. The actual errors do not agree with the predicted errors, although there are some similarities. The actual errors appear arbitrary, perhaps reflecting inaccuracies in the applied load as much as inherent inaccuracy of the transducer itself. If the predicted errors are used to 'correct' the measured errors, there is no general improvement. The RMS errors of the 69 test loads after correction are given in Table 9. These should be compared with the uncorrected values in Table 8.

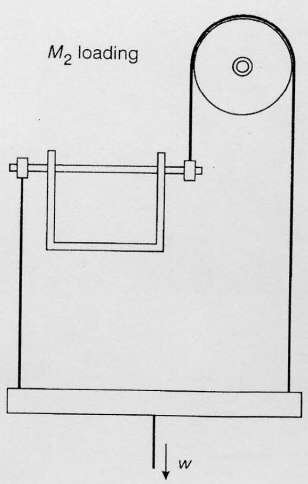

Fig. 8 *Schematic diagram of M_2 loading*

Table 9 RMS values of six errors averaged over all 69 tests after 'correction' using theoretical effects of transducer's compliance

F_1	F_2	F_3	M_1	M_2	M_3
1.27 N	2.55 N	1.92 N	0.58 Nm	0.62 Nm	0.78 Nm

If we had found good agreement between the actual errors and the theoretical errors due to compliance, we would have used this theory as an error predictor. One advantage would then have been that the errors would have increased with load (albeit non-linearly), and therefore the expected fractional errors under light loading would not have been great. As, in fact, the compliance theory does not account for the errors, the next question, given that we need to be able to propagate the errors from the transducer measurements to the joint moments (WOOD *et al.*, 1999), is to discover whether the errors are systematic or random.

Table 10 shows the correlation coefficients between the errors for the 69 loads in Table 7. To assess whether these are random, Table 11 shows the probability of these correlation coefficients occurring if the errors are random and normally distributed (TAYLOR, 1982) (Appendix C).

Because a few of these figures are not small, these pairs of errors may be uncorrelated, but, for most pairs, the correlations are significant (5%) or highly significant (1%). We conclude that, for error propagation, the errors may be correlated and therefore should not be added in quadrature (TAYLOR, 1982) (p. 178). The standard deviation for the six errors are the RMS values in Table 7.

5.3 *Measurement range*

To assess the measurement range of the transducer, we can imagine loading with each of the six forces or moments alone. Then, with the amplifier gains given, the greatest measurable load occurs when one amplifier saturates. Taking the largest coefficient in each column of $\boldsymbol{K}_{calib}$ and dividing these into the maximum input to the A–D converters (2.5 V), we obtain the loads given in Table 12. Generally, with combined loads, the maximum measured loads at which one A–D converter saturates will be lower.

6 Review of the six-axis transducer design

If non-linear behaviour due to the transducer compliance introduced significant error, this transducer could be improved by using beams of greater section, except at the gauge sites, stiffer clamps and a stiffer footbox crutch. However, at present, these results suggest that the errors (meaning the measurable errors rather than errors that are inherent in the transducer itself) are systematic, because they are correlated, but apparently arbitrary, as they are not described by the compliance

Table 10 Correlation coefficients between six components of error during 69 load tests

	F_1	F_2	F_3	M_1	M_2	M_3
F_1	1.00					
F_2	0.43	1.00				
F_3	−0.04	0.48	1.00			
M_1	0.38	0.30	0.40	1.00		
M_2	−0.21	−0.26	−0.15	−0.47	1.00	
M_3	−0.44	−0.43	−0.21	0.22	−0.15	1.00

Table 11 Probabilities of correlations in Table 10 occurring

	F_1	F_2	F_3	M_1	M_2	M_3
F_1	0					
F_2	<0.1%	0				
F_3	68%	<0.1%	0			
M_1	0.2%	1.2%	<0.1%	0		
M_2	~9%	~3%	22%	<0.1%	0	
M_3	<0.1%	<0.1%	~8%	~7%	22%	0

Table 12 Greatest measurable load when all other components are zero

F_1	F_2	F_3	M_1	M_2	M_3
808 N	651 N	352 N	134 Nm	94 Nm	225 Nm

theory of the Appendix or any other known theory. Perhaps these are due to inaccuracy in the loading arrangements during calibration and validation.

In this design, we chose to measure force in a way that is easy to implement: measuring the difference in the bending moments along a transversely loaded beam. As this necessitates increasing the error, a fundamentally better method is to measure the shear strain in the web of an I-section beam, which varies directly with the force. This will make the $\boldsymbol{G}$ matrix more diagonally dominant, and therefore the calculations will be better conditioned.

The most critical property of the MMCS is the accuracy with which it can measure the joint moments, which depends on the accuracy of the six-axis transducers. We assess the performance of the transducer in this application at the end of Part 2 (WOOD *et al.*, 1999).

References

BOYLE, H. B. (1992): 'A balancing act: a multi component force balance primer', *in* LITTLE, E. G. (Ed): 'Experimental mechanics' (Elsevier) pp. 353–364

BRINDLEY, G. S., POLKEY, C. E., and RUSHTON, D. N. (1979): 'Electrical splinting of the knee in paraplegia', *Paraplegia*, **16**, pp. 428–435

BRINDLEY, G. S. (1995): 'The first 500 sacral anterior root stimulator implants - implant failures and their repair', *Paraplegia*, **33**, pp. 5–9

CARPENTER, R. H. S. (1996): 'Neurophysiology, 3rd edn.', (Arnold) p. 215

DAVIES, R., HOUDAYER, T., ANDREWS, B., PATRICK, J., and MORTLOCK, A. (1995): 'Hybrid standing with the Cochlear FES-22 stimulator and Andrews FRO brace', Proc. 5th Vienna Int. Workshop on Functional Electrostimulation, pp. 55–58

DONALDSON, N. (1986): 'A 24-output implantable stimulator for FES'. Proc. 2nd Vienna Int. Workshop on Functional electrostimulation, pp. 197–200

GRAY (1989): 'Gray's anatomy, 37th edn: WILLIAMS, WARWICK, DYSON and BANNISTER (Eds), Churchill Livingstone, Edinburgh

HAMSTER, A. A. (1995): 'Analysis of muscle responses to lumbosacral nerve root stimulation'. M.Sc. thesis (Bio 95-21) University of Twente, Institute of Biomedical Technology

LIGUORI, R., KRARUP, C., and TROJABORG, W. (1992): 'Determination of the segmental sensory and motor innervation of the lumbosacral spinal nerves', *Brain*, **115**, 915–934

PERRY, C. C., STARR, J. E., and WEIDNER, J. R. (1992): 'Modern strain transducers: their design and construction', *in* HANNAY, R. L., and REED, S. E. (Eds.): 'Strain gauge users handbook' (Soc. for Experimental Mechanics Inc., Elsivier Applied Science) ISBN 1-85166-686-9

RUSHTON, D. N. (1990): 'Choice of nerves or roots for multichannel leg controller implant', *in* POPOVIC, D. (Ed.): 'Advances in the

external control of human extremities X' (Nauka, Belgrade) pp. 177–187

SHELL, D. (1990): 'High-accuracy bridge amplifier', *Electron. Wirel. World*, July, pp. 582–583

TAYLOR, J. R. (1982): 'An introduction to error analysis' (University Science Books (distributed by OUP outside USA)) ISBN 0 19 855707-8, Appendix C

THOMA, H., FREY, M., GRUBER, H., HOLLE, J., KERN, H., REINER, E., SCHWANDA, G., and STOHR, H. (1983): 'First implantation of a 16-channel electric stimulation device in the human body', *Trans. Am. Soc. Artif. Organs*, **XXIX**, pp. 301–306

WILEMON, W. K., MOONEY, V., MCNEAL, D. and RESWICK, J. (1970): 'Surgical implanted peripheral neuroelectric stimulation'. Internal Report, Rancho Los Amigos Hospital, Downey, California

WOOD, D. E., DONALDSON, N. de N. and PERKINS, T. A. (1999): 'Apparatus to measure simultaneously 14 isometric leg joint moments. Part 2: Multi-moment chair system', *Med. Biol. Eng. Comput.*, **37**, 148–154

YOUNG, W. C. (1989): 'Roark's formulas for stress and strain, 6th edn.' (McGraw-Hill International)

Appendix: Errors due to deflections of the transducer

Owing to the finite stiffness of the transducer, loading causes deflections at the load (ankle axis). These deflections are both translations and rotations. The translations do not affect the measured forces and moments, but the effect of the rotations is to misalign the transducer axes with the ground axes. If the rotations are θ_1, θ_2 and θ_3, clockwise about the three axes, the effect of applying them in order is $\boldsymbol{R}$

$$\boldsymbol{R} = \begin{bmatrix} 1 & \theta_3 & 0 \\ -\theta_3 & 1 & 0 \\ 0 & 0 & 1 \end{bmatrix} \cdot \begin{bmatrix} 1 & 0 & -\theta_2 \\ 0 & 1 & 0 \\ \theta_2 & 0 & 1 \end{bmatrix} \cdot \begin{bmatrix} 1 & 0 & 0 \\ 0 & 1 & \theta_1 \\ 0 & -\theta_1 & 1 \end{bmatrix} \tag{16}$$

where, because the angles are small, the approximations $\sin(\theta) \approx \theta$ and $\cos(\theta) \approx 1$ have been applied. Multiplying out and neglecting θ products,

$$\boldsymbol{R} = \begin{bmatrix} 1 & \theta_3 & -\theta_2 \\ -\theta_3 & 1 & \theta_1 \\ \theta_2 & -\theta_1 & 1 \end{bmatrix} \tag{17}$$

which is independent of the order of multiplication. Thus, if forces $[F_1, F_2, F_3]$ are applied referred to the ground axes, the apparent forces, referred to the transducer axes, will be

$$\begin{bmatrix} F'_1 \\ F'_2 \\ F'_3 \end{bmatrix} = \boldsymbol{R}. \begin{bmatrix} F_1 \\ F_2 \\ F_3 \end{bmatrix} \tag{18}$$

Therefore the errors are

$$\begin{bmatrix} F'_1 \\ F'_2 \\ F'_3 \end{bmatrix} - \begin{bmatrix} F_1 \\ F_2 \\ F_3 \end{bmatrix} = \begin{bmatrix} \Delta F_1 \\ \Delta F_2 \\ \Delta F_3 \end{bmatrix} = (\boldsymbol{R} - \boldsymbol{I}) \begin{bmatrix} F_1 \\ F_2 \\ F_3 \end{bmatrix} \tag{19}$$

where $\boldsymbol{I}$ is the unit matrix. Similarly, for the moments,

$$\begin{bmatrix} M'_1 \\ M'_2 \\ M'_3 \end{bmatrix} - \begin{bmatrix} M_1 \\ M_2 \\ M_3 \end{bmatrix} = \begin{bmatrix} \Delta M_1 \\ \Delta M_2 \\ \Delta M_3 \end{bmatrix} = (\boldsymbol{R} - \boldsymbol{I}) \begin{bmatrix} M_1 \\ M_2 \\ M_3 \end{bmatrix} \tag{20}$$

The rotations are caused by the load forces and moments. In general,

$$\begin{bmatrix} \theta_1 \\ \theta_2 \\ \theta_3 \end{bmatrix} = \begin{bmatrix} \alpha_{11} & \alpha_{12} & \alpha_{13} \\ \alpha_{21} & \alpha_{22} & \alpha_{23} \\ \alpha_{31} & \alpha_{32} & \alpha_{33} \end{bmatrix} \begin{bmatrix} F_1 \\ F_2 \\ F_3 \end{bmatrix} + \begin{bmatrix} \beta_{11} & \beta_{12} & \beta_{13} \\ \beta_{21} & \beta_{22} & \beta_{23} \\ \beta_{31} & \beta_{32} & \beta_{33} \end{bmatrix} \begin{bmatrix} M_1 \\ M_2 \\ M_3 \end{bmatrix} \tag{21}$$

However, by considering the symmetries of the transducer, we see that most of these compliances are zero

$$\begin{bmatrix} \theta_1 \\ \theta_2 \\ \theta_3 \end{bmatrix} = \begin{bmatrix} 0 & 0 & \alpha_{13} \\ 0 & 0 & \alpha_{23} \\ \alpha_{31} & \alpha_{32} & 0 \end{bmatrix} \begin{bmatrix} F_1 \\ F_2 \\ F_3 \end{bmatrix} + \begin{bmatrix} \beta_1 & 0 & 0 \\ 0 & \beta_2 & 0 \\ 0 & 0 & \beta_3 \end{bmatrix} \begin{bmatrix} M_1 \\ M_2 \\ M_3 \end{bmatrix} \tag{22}$$

To measure the compliances, a laser pointer was taped to the transducer during loading, and the deflection of the spot on the wall was observed. The compliances are

$$\alpha_{13} = 0.0132 \times 10^{-3} \text{ rad N}^{-1}$$
$$\alpha_{23} = -0.0872 \times 10^{-3} \text{ rad N}^{-1}$$
$$\alpha_{31} = 0.0048 \times 10^{-3} \text{ rad N}^{-1}$$
$$\alpha_{32} = 0.0668 \times 10^{-3} \text{ rad N}^{-1}$$
$$\beta_1 = 0.279 \times 10^{-3} \text{ rad Nm}^{-1}$$
$$\beta_2 = 0.236 \times 10^{-3} \text{ rad Nm}^{-1}$$
$$\beta_3 = 0.230 \times 10^{-3} \text{ rad Nm}^{-1}$$

With these, and for any loading, the deflections can be calculated with eqn. 22, and the rotations can be substituted into eqns. 19 and 20 to find the moment errors.

Although it is neatest, in a program, to calculate the angles first and, from them, the errors, it is interesting to substitute the deflection expressions into eqns. 19 and 20. For example, for eqn. 19,

$$\begin{bmatrix} \Delta F_1 \\ \Delta F_2 \\ \Delta F_3 \end{bmatrix} = \begin{bmatrix} \alpha_{31} F_1 F_2 + \alpha_{32} F_2^2 + \beta F_2 M_3 - \alpha_{23} F_3^2 - \beta_2 F_3 M_2 \\ -\alpha_{31} F_1^2 - \alpha_{31} F_1 F_2 - \beta_3 F_1 M_3 + \alpha_{13} F_3^3 + \beta_1 F_3 M_1 \\ \alpha_{23} F_1 F_3 + \beta_2 F_1 M_2 - \alpha_{13} F_2 F_3 - \beta_1 F_2 M_1 \end{bmatrix} \tag{23}$$

showing how the errors depend on terms that are the sums of products of the applied forces and moments.

Authors' biographies

NICK DONALDSON obtained his MA in engineering from Cambridge University, in 1976. He joined the Medical Research Council Neurological Prostheses Unit. Since then, he has worked on the use of surgically implanted devices for restoring paralysed limb function. Since 1992, he has been Head of the Implanted Devices Group at University College London. His research interests include implant technology, implanted orthopaedic instrumentation, the biomechanics of standing, biomechanical instrumentation, nerve and nerve root stimulation, feedback control in FES, and use of ENG signals in control.

MARKO MUNIH received his BSc in 1986, and an MSc in Electrical Engineering from the University of Ljubljana, Slovenia, in 1989. He received a DSc degree in Electrical Engineering in 1993, for work on controlling muscle activity with respect to the femur and tibia bone loading. From 1989, he was Teaching Assistant at the Faculty of Electrical Engineering, Ljubljana, Slovenia. His research interests included functional electrical stimulation of paraplegic lower extremities with surface electrode systems. From 1995 to 1996, he was Research Assistant with the Implanted Devices Group, at University College London. Currently, he is a faculty member at the Faculty of Electrical Engineering, University of Ljubljana, Slovenia.

TIM PERKINS obtained a BSc in Physics from Bristol University in 1971, and an MSc in Electrical Engineering from Chelsea College, in 1982. He joined the MRC Neurological Prostheses Unit, in 1972, where he specialised in designing the external control circuitry for RF inductively coupled implants. Among the stimulation controllers he developed were those for restoration of leg function in paraplegia (using femoral nerve stimulation), hand function in tetraplegia, cochlea stimulation for the profoundly deaf and bladder and bowel control in the spinal injured via sacral anterior root stimulation implants. For the latter, he was joint winner of the IEE prize for helping disabled people in 1985. In 1992, he moved to University College London.

DUNCAN WOOD obtained his BEng in 1989, in Electronic Engineering, from the University of Southampton, and his MSc in 1990, and PhD in 1995, in Biomedical Engineering, from the University of Surrey. He is currently at Salisbury District Hospital, working as a clinical engineer on functional electrical stimulation (FES) programs to correct neurological disorders. His main role is providing a program that uses electrical stimulation to assist paraplegics to stand. Other research interests include using FES to correct gait disorders or hand dysfunction, the measurement of spasticity, and the measurement of EMG signals as a control of stimulation patterns.